MATERIALS CHEMISTRY FRONTIERS

CCS 中国化学会 CHINESE CHEMICAL SOCIETY

ICCAS

ROYAL SOCIETY OF CHEMISTRY

Substituent dependent deep-blue pyrene-based chemosensor for trace nitroanilines sensing

Journal:	*Materials Chemistry Frontiers*
Manuscript ID	QM-RES-04-2023-000342.R1
Article Type:	Research Article
Date Submitted by the Author:	20-Apr-2023
Complete List of Authors:	Li, Hua-Long; Shandong University of Technology, School of Chemical Engineering Cao, Jing-Yi; Shandong University of Technology, School of Chemical Engineering Yu, Ze-Dong; Shandong University of Technology, School of Chemical Engineering Yang, Guang; Shandong University of Technology, Chemical Engineering Xue, Zeng-Min; Shandong University of Technology, School of Chemical Engineering Wang, Chuan-Zeng; Shandong University of Technology, School of Chemistry and Chemical Engineering Zhao, Wen-Xuan; Shandong University of Technology, School of Chemistry and Chemical Engineering Zhao, Yi; Shandong University of Technology Redshaw, Carl; University of Hull Scarborough Campus, Department of Chemistry Yamato, Takehiko; Saga University, Department of Chemistry and Applied Chemistry

Substituent dependent deep-blue pyrene-based chemosensor for trace nitroanilines sensing

Received 00th January 20xx,
Accepted 00th January 20xx

DOI: 10.1039/x0xx00000x

Hua-Long Li,‡[a] Jing-Yi Cao,‡[a] Ze-Dong Yu,[a] Guang Yang,[a] Zeng-Min Xue,[a] Chuan-Zeng Wang*[a,b] Wen-Xuan Zhao,[a] Yi Zhao,*[a] Carl Redshaw[c] and Takehiko Yamato,*[b]

Nitroaniline (**NA**) is a kind of high toxicity and pathogenic amine derivatives, and the trace monitoring of nitroaniline has become an urgent problem in the field of environment and security. Herein, two K-region multiple substituted pyrene-based luminogens with reasonable photoluminescence efficiency and blue emission (408–430 nm) have been synthesized and characterized. Their photophysical properties were carefully investigated in solution and in the solid state by experimental and density functional theory (DFT) methods. It is worth mentioning that both these π-electron rich and extended π-conjugated materials were used for the detection of electron deficient nitroaromatics (**NACs**) based on photo-induced electron transfer (PET) mechanism, and a sensitive response towards **NA**, especially for ***p*-NA** with a limit of detection (LOD) as low as 8.58×10^{-9} M was observed, and the fluorescence quenching efficiency up to 99.5%. These research results provided a low-cost and simple strategy for trace nitroanilines sensing.

Introduction

Nitroaromatic compounds are indispensable chemicals in industry，and are widely utilized in the production of pesticide, medicine, dye, chemical fiber and rubber and other products.[1–3] On the other hand, the use of nitro-explosives also reveals their negative impact on human health, environment and national security.[4–7] In this context, a variety of methods have been established for explosive detection with a fast response time, super-sensitivity and ultra-selectivity, such as Raman spectroscopy, thermal neutron analysis, gas chromatography-electron capture detection and ion mobility spectroscopy.[8–11] However, traditional methods expose significant disadvantages, including long time-dependence for recognition, complexity of sample preparation and high cost. Given the urgency of the portability and sensitivity for detection, fluorescence detection of nitro-explosives by exploring the luminescence properties of luminogents has been widely investigated, including luminescent nitrogen-doped graphene quantum dots,[12] metal cluster decorated graphene nanoflakes,[1,13–15] metal organic frameworks,[16,17] covalent organic frameworks and conjugated polymers.[18–20] In sharp contrast, different from the complex preparation procedure of the fluorescence sensing materials mentioned above, fluorescent small molecules have been widely used as efficient fluorescence sensors due to their excellent molar absorption, high quantum efficiency and amplified sensing response.[21,22] Thus, the synthesis of high efficiency fluorescent small organic molecules remains a hot research topic. The luminescence sensing mechanisms mainly include donor–acceptor electron transfer (ET),[23,24] resonance energy transfer (RET),[25] inner filter effect (IFE)[26] and absorption competition quenching.[27] Generally speaking, all of the above mechanisms can be employed to interpret the fluorescence turn-off/turn-on phenomena for sensing applications.

Pyrene, as a typical and quality fluorophore, has been widely used in many fields, ranging from optoelectronics, stimuli-responsive system, bioimaging to chemosensing.[28] Such wide application is mainly attributed to its desirable properties, such as being amenable to controllable regio-selective functionalization, having a high thermal stability, enhanced charge carrier mobility and high luminescence efficiency. Various controllable regio-selective synthetic strategies based on the multi-active sites of the pyrene core have been established.[29–36] Moreover, a series of pyrene-based blue-emitting materials exhibited excellent recognition performance towards nitroanilines due to the large overlap between the absorption of nitroanilines and emission spectra of pyrene-based luminogens.[37,38] And K-region of pyrene core were highly considered as functional sites based on extensive reported of blue-emitting pyrene derivatives previously.[29,30]

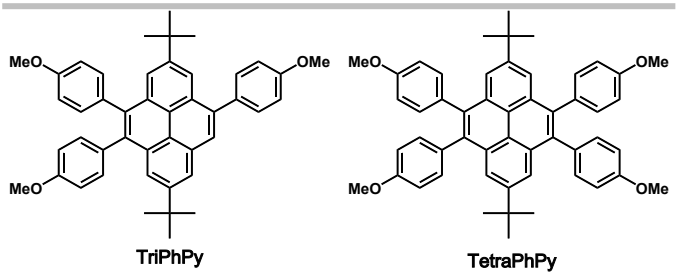

Scheme 1. Chemical structures of **TriPhPy** and **TetraPhPy**.

[a] *School of Chemistry and Chemical Engineering, Shandong University of Technology, Zibo 255049, P. R. China*
[b] *. Department of Applied Chemistry, Faculty of Science and Engineering, Saga University Honjo-machi 1, Saga 840-8502 Japan*
[c] *Chemistry, School of Natural Sciences, The University of Hull, Cottingham Road, Hull, Yorkshire HU6 7RX, UK.*

‡ H.-L. L and J.-Y. C. contributed equally to this work. The authors declare no competing financial interest.

Electronic Supplementary Information (ESI) available: [details of any supplementary information available should be included here]. See DOI: 10.1039/x0xx00000x

In the present work, two pyrene-based luminogens have been prepared by a controllable functionalization approach at the K-region (Scheme 1). The two derivatives **TriPhPy** and **TetraPhPy** present similar photophysical properties with short wavelength emission in the near-ultraviolet region. Interestingly, distinct sensitivities between **TriPhPy** and **TetraPhPy** for the detection of nitroaniline (**NA**) isomers were observed. Thus, an efficient substituent-dependent near-ultraviolet pyrene-based chemosensor for trace nitroanilines (LOD as low as 8.58×10^{-9} M) is demonstrated.

Results and discussion

Synthesis and characterization

During our attempts to synthesize K-region tetrasubstituted pyrene-based derivatives as extended aromatic systems, we have unexpectedly obtained another tribromo-substituted intermediate through a "one-pot" process. As depicted in Scheme S1, the intermediates **TriBrPy** and **TetraBrPy** were synthesize starting from 2,7-di-*tert*-butylpyrene[39] by a regular bromination reaction. The ratio of 1:9 of both intermediates were clearly calculated by ^{1}H NMR spectroscopic results (a consistent ratio was obtained by integration based on the pyrene moiety and *tert*-butyl groups as shown in Fig. S1, ESI‡). Thus, the substituent dependent pyrene-based luminogens **TriPhPy** and **TetraPhPy** were further synthesized *via* Suzuki crossing coupling in one pot. These two products could readily be separated by column chromatography and recrystallization in reasonable yields, and unambiguously charactered by ^{1}H NMR/^{13}C NMR spectroscopy and by high resolution mass spectrometry (Fig. S2–5, ESI‡).

Photophysical properties

The UV-Vis absorption and emission properties of the luminogens **TriPhPy** and **TetraPhPy** in dilute organic solutions and in the solid state were studied, and partial parameters are listed in Table 1. The absorption spectra of the two luminogens in DCM both reveal two absorption bands of different shapes (Fig. 1A). Specifically, similar intense absorption band at around at 295 nm are ascribed to the locally excited (LE) state of the pyrene core, and another set of moderate shoulder absorption bands, which are centered at 338 nm and 353 nm correspond to π-π* transitions of the pyrene core and peripheral substituents. In contrast, a weak absorption were observed for **TetraPhPy** in the range of 375~400 nm, which should be attributed to the CT transition from more peripheral substituents to pyrene core than **TriPhPy**.[40]Furthermore, possible solvatochromic effects were investigated in different organic solvents (dimethylformamide (DMF), dichloromethane (DCM), tetrahydrofuran (THF), 1,4-dioxane, and cyclohexane) of various polarities (Fig. S6–7, ESI‡). The maximum absorption wavelengths remain almost constant for the low energy absorption band (338 nm and 353 nm for **TriPhPy** and 338 nm and 353 nm for **TetraPhPy**) and the high energy absorption band (293 nm for **TriPhPy** and 295 nm **TetraPhPy**) in both molecular systems.

Table 1. The photophysical properties of **TriPhPy** and **TetraPhPy**

Compounds	λ_{abs}(nm) sol[a]	λ_{em}(nm) sol[b] / solid	Φ_{FL}[c] (%) sol[a] / solid	HOMO[d] (eV)	LUMO[d] (eV)	ΔE_g[d] (eV)
TriPhPy	293, 353	408 / 412	30.6 / 1.2	−5.00	−1.31	3.69
TetraPhPy	295, 353	413 / 430	61.3 / 6.5	−4.90	−1.20	3.70

[a] 1×10^{-5} M in CH_2Cl_2, λ_{abs} is the absorption band appearing at the longest wavelength.

[b] 1×10^{-7} M in CH_2Cl_2, λ_{em} is the fluorescence band appearing at the shortest wavelength.

[c] Absolute quantum yield (±0.01−0.03).

[d] DFT/B3LYP/6-31G* using Gaussian.

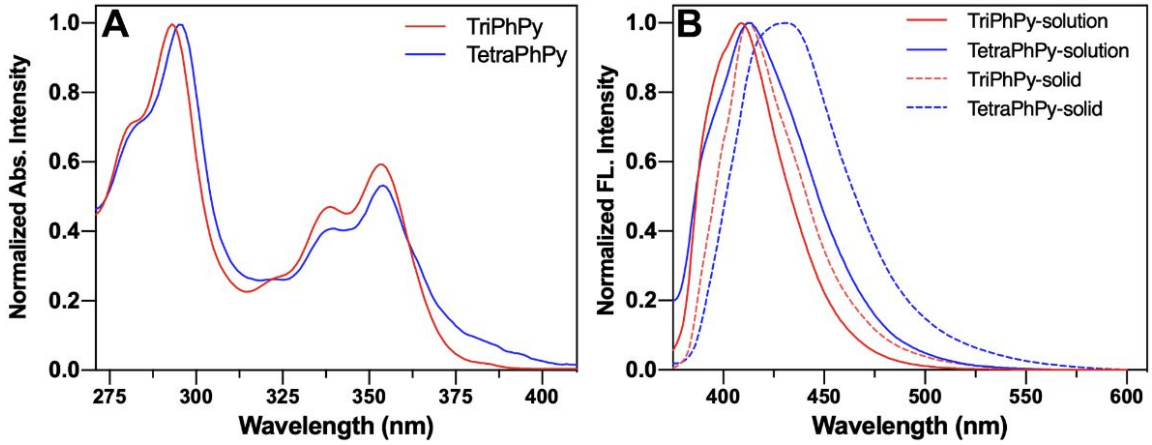

Fig. 1. UV-Vis absorption **(A)** and emission spectra (B) for **TriPhPy** and **TetraPhPy** in DCM solution and in the solid state, respectively.

The fluorescence spectra of these two compounds were recorded in both DCM solution and in the solid state. As shown in Fig. 1B, similar emission behavior around λ_{max} = 408 nm and 413 nm corresponding to **TriPhPy** and **TetraPhPy** were observed, respectively, which are attributed to the monomer emission of the pyrene core. In terms of absorption behavior, the peripheral substituent groups just show a weak influence on their emission characteristics in dilute organic solution, which can be attributed to the extended π conjugation for **TetraPhPy** with four aryl substituents than **TriPhPy** with three groups. Interestingly, a significant difference in the emission spectra was present in the solid state, for **TriPhPy**, the maximum emission wavelength is 412 nm, which is almost same as in solution. On the other hand, **TetraPhPy** reveals a distinct red-shift with 18 nm relative to the luminogen **TriPhPy**, which may be ascribed to the influence of the difference of the molecular arrangement and intermolecular interactions due to the different number of substituents.[41]

A detailed investigation of the solvatochromic effects of both luminogens in different organic solvents with various polarities was performed, which can effectively elucidate the luminescence mechanism by comparing the photophysical properties in different states. As shown in Fig. S8 and Fig. S9, ESI‡, a set of almost identical maximum emission wavelengths centered at 408 nm for **TriPhPy** from cyclohexene to DMF were observed, while a small blue-shift (2 nm) for **TetraPhPy** from cyclohexene to DMF was present. These solvatochromic results indicate that a locally excited LE emission plays a dominant role in dilute solutions. An in-depth study of the emission properties of these two luminogens was performed based on the CIE 1931 chromaticity diagram. All the luminescence color coordinates of the two luminogens in different diluted organic solutions are concentrated in a small area (CIE: x < 0.163, y < 0.021 for **TriPhPy**, and x < 0.158, y < 0.032 for **TetraPhPy**). These results further indicate that the stability of the luminescence properties is independent of the solvent polarity.[42,43]

To further evaluate the luminogen properties, the absolute fluorescence quantum yields (Φ_{FL}) were investigated. As compared with the emission properties in diluted solution and in the solid state, the absolute fluorescence quantum yields exhibited a marked difference in the different states. Both luminogens exhibit higher values for Φ_{FL} in DCM solution (30.6% for **TriPhPy**, 61.3% for **TetraPhPy**), while a dramatically reduced Φ_{FL} was observed in the solid state (1.2% for **TriPhPy**, 6.5% for **TetraPhPy**), which can be attributed to the different molecular arrangements and intermolecular interactions based on the number of peripheral substituents in the aggregated state. Specifically, the different intermolecular interactions triggered disparate supramolecular structures making different contributions for dissipating the exciton energy as a non-radiative pathway in the aggregates.[44] Overall, the substituent dependent pyrene-based luminogens provide an efficient design strategy for deep-blue emitters.

In order to further elucidate the structure-activity relationship, theoretical explorations were carried out at the B3LYP/6-31g-(d) level.[45,46] Generally, the distributions of their highest occupied molecular orbital (HOMO) and lowest unoccupied molecular orbital (LUMO) largely reflect the ability of electron-donating/electron-withdrawing of peripheral substituents at the K-region.[33,43] As shown in Fig. 2, minimal differences of frontier-molecular-orbital distributions and energy gaps (ΔE_g) between **TriPhPy** (3.69 eV) and **TetraPhPy** (3.70 eV) were observed. The distributions of HOMO and LUMO for both two luminogens are mainly located over the pyrene core, almost identical results are consistent with the aforementioned absorption properties. However, such DFT calculation results are somewhat inconsistent with the emission properties, especially in the solid state, which should be attributed to the absence of evaluation of intermolecular interactions in the theoretical calculation.[47]

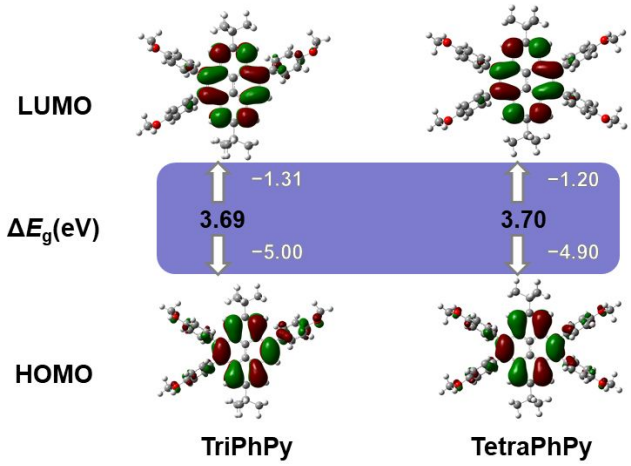

Fig. 2. Frontier-molecular-orbital distributions and energy level diagrams for **TriPhPy** and **TetraPhPy** by DFT calculations.

The morphology of both compounds was further investigated using scanning electron microscopy (SEM). As can be seen from Fig. 3, the morphology of the two materials exhibited obvious differences. The microstructure of **TriPhPy** (A and B) is characterized by a sheet structure with lengths of up to tens of microns, while **TetraPhPy** (C and D) exhibited a rod-like distribution with about 5 to 10 microns in length, which may be due to differences of the molecular arrangement in the solid state. This results also provide convincing evidence for the difference of absolute fluorescence quantum yields in the solid state.[48]

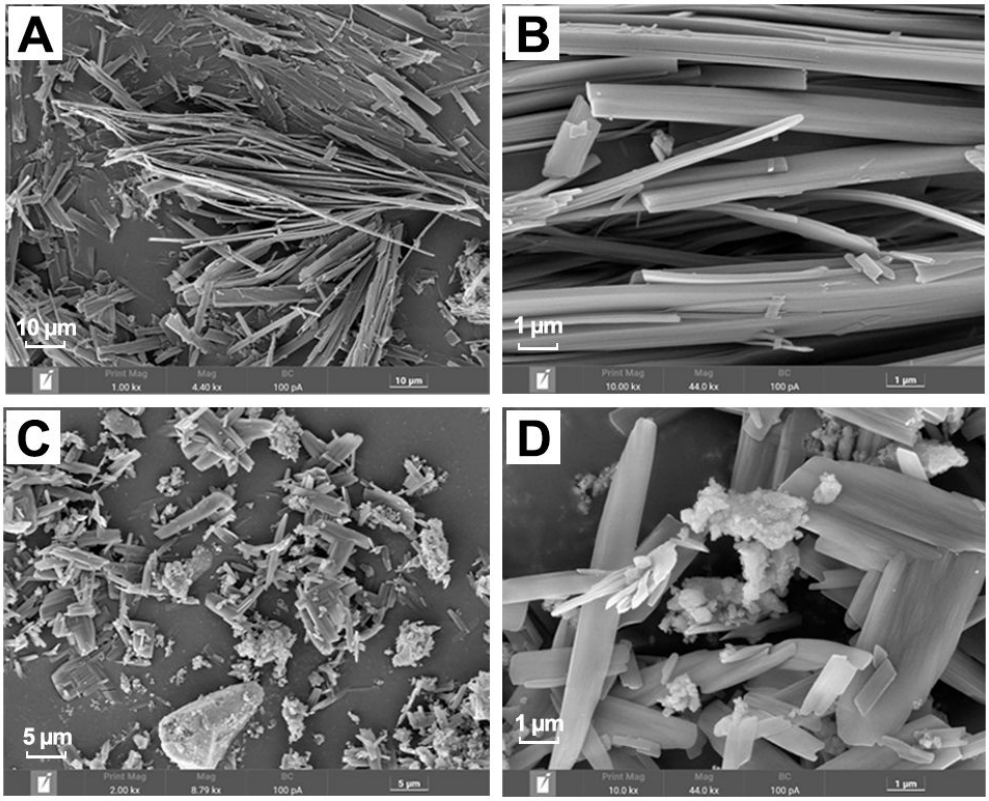

Fig. 3 SEM microphotographs of powdered **TriPhPy** (A and B) and **TetraPhPy** (C and D) at different magnification, respectively.

Detection of nitroaniline

The relatively similar photophysical properties, especially in solution, motivated us to further investigate selectivity and differentiation in practical applications. In this system, π-electron rich and extended π-conjugated structures were synthesized by introducing multiple electron-donating aryls, which are promising candidates as chemosensors for the detection of electron deficient nitroaromatics (**NACs**) based on a photo-induced electron transfer (PET) mechanism.[49]

Considering the above characteristics of the absorption spectra of **NA** and fluorescence spectra of these two luminogens (Fig. 4A), a series of systematic investigations were carried out to detect nitroanilines by testing standard DCM solutions containing different concentrations of **NA** which varied from 0.2 to 1.2 mmol L^{-1} (Fig. S10–14 ESI‡). Taking **TriPhPy** and ***p*-NA** as an example, as shown in Fig. 4B, a remarkable quenching was observed with increasing concentration of ***p*-NA** and the luminescence quenching efficiency is up to 99.7%, which is comparable to or even better than previously reported pyrene-based sensors in nitro-explosives detection field.[37,38] Accordingly, for ***m*-NA** and ***o*-NA**, relatively weak quenching results (82.4% for ***m*-NA** and 97.8% for ***o*-NA**) for **TriPhPy** were recorded. Such results revealed a good selectivity for the detection of the isomers of nitroaniline. Moreover, similar quenching and selectivity for the luminogen **TetraPhPy** was observed, and the values of luminescence quenching efficiency were found to be 99.5% for ***p*-NA**, 90.6% for ***m*-NA** and 98.5% for ***o*-NA**, respectively. Both luminogens exhibit excellent selectivity and sensitivity for ***p*-NA** as a chemosensor, especially **TriPhPy**. More visual histograms present the differences in quenching selectivity and sensitivity as shown in Fig. 4C and Fig. S15 ESI‡. The detection efficiency of these two materials was further confirmed by a hyperbolic curved Stern–Volmer plot by the Stern–Volmer (SV) equation and the limit of detection by equation: LOD = $3\sigma/K$. As shown in Fig. 4D and the inset photograph, a curved Stern–Volmer plot in the whole concentration system (up to 1.2 mM) and a linear Sterne-Volmer plots at lower concentration (up to 0.6 mM) of ***p*-NA** *versus* the fluorescence intensity, which may be ascribed to the synergistic effect of dynamic and static quenching mechanism for former and a static quenching mechanism for latter.[50] The Stern–Volmer constant (K_{sv}) of 1.61×10^4 M^{-1} and a LOD of 8.58×10^{-9} M were calculated for the **TriPhPy**/***o*-NA** system. The detailed calculation procedure and results for other **TriPhPy**/**NA** and **TetraPhPy**/**NA** systems are shown in the standard deviation and detection limit calculations part of the supporting information. The experimental results revealed that these materials with efficient and sensitive quenching response for **NA** are promising pyrene-based chemosensor based on the PET mechanism.[51]

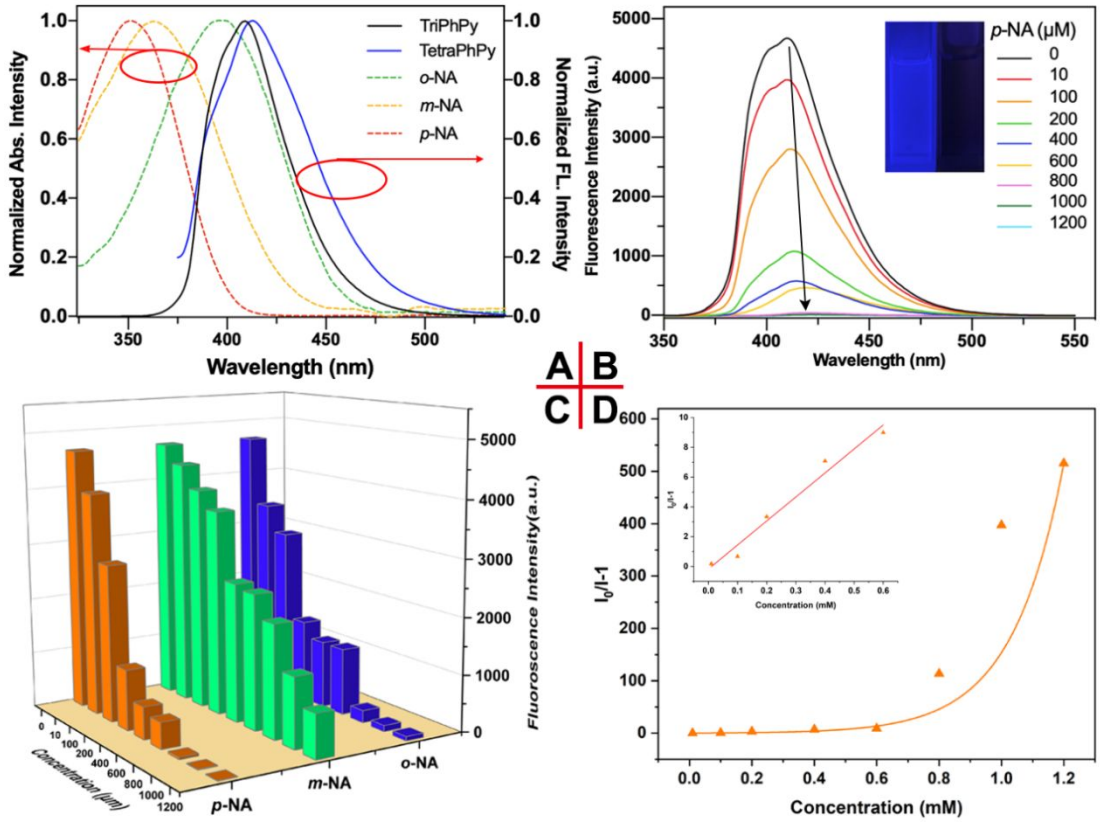

Fig. 4. (A): Normalized absorption spectra of **NA** and fluorescence spectra of two luminogens in DCM; (B): Fluorescence quenching of **TriPhPy** on incremental addition of ***p*-NA** and inset photographs show the visible change in the fluorescence under UV light before and after addition of ***p*-NA**; (C): Histogram of the fluorescence quenching of **TriPhPy** with **NA**; (D): Corresponding Sterne-Volmer plots for quenching of **TriPhPy** with ***p*-NA** as quencher in DCM. Inset shows the Sterne-Volmer plots at lower concentration of ***p*-NA**.

A more practical study was carried out by preparing portable test strips. Specifically, the test strips were prepared by dip coating a DCM solution of **TriPhPy** onto qualitative filter paper followed by drying under vacuum. Then a series of solutions of nitroaniline isomers at different concentration from 10^{-12} M to 10^{-2} M were dripped onto the prepared test strips. As shown in Fig. 5, significant quenching phenomenon was observed even by adding tiny drops at low concentrations (8 μL of 10^{-12} M) of nitroanilines under 365 nm UV irradiation. A visual detection result for trace nitroanilines consistent with the above fluorescence quenching results in solution was observed, and an efficient and portable visual fluorimeter for trace nitroanilines sensing is expected to be developed and go into service, particularly for *para*-nitroaniline in the future.

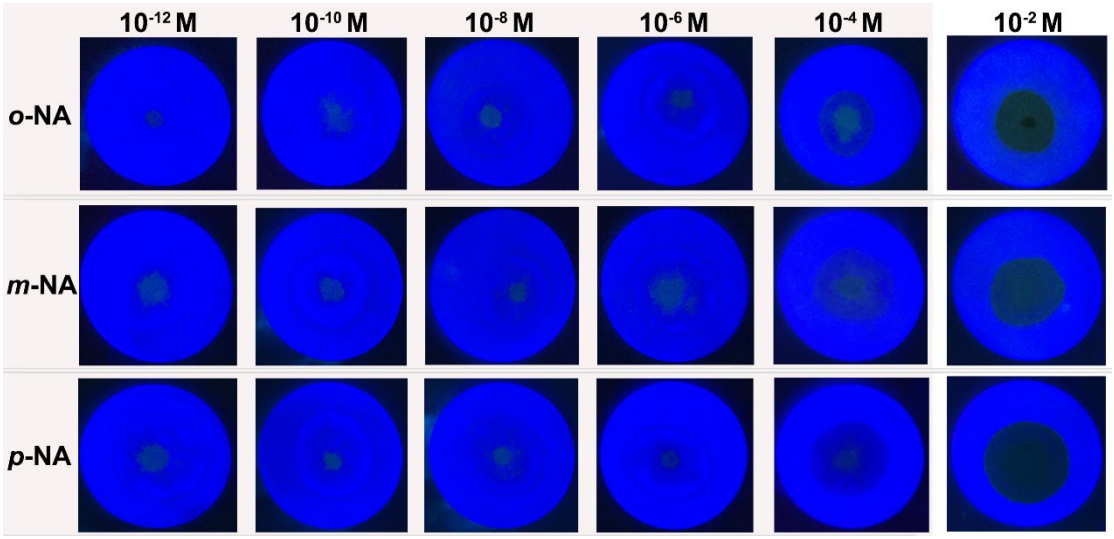

Fig. 5. Test strips of **TriPhPy** and its response to **NA** at different concentrations under UV irradiation.

Conclusions

In summary, two K-region multiple substituted pyrene-based luminogens with π-electron rich and electron-donating groups were prepared. The peripheral substituent number dependent materials encouraged us to explore the sensing properties for the detection of trace nitroaniline (**NA**), including ***p*-NA**, ***m*-NA** and ***o*-NA**. The experimental results revealed that luminogens **TriPhPy** and **TetraPhPy** exhibited excellent sensitivity and selectivity particularly for ***p*-NA** with a competitive detection limit as low as 10^{-9} M. Moreover, the visual detection exhibited excellent sensitivity by employing portable test strips, and an obvious quenching phenomenon was observed even by just dropping an 8 μL dilute solution of concentration of 10^{-12} M. Thus, this work provides an efficient and convenient strategy for the visual detection of trace nitroanilines sensing by constructing K-region substituted pyrene-based luminogens.

Experimental

All reagents were purchased from commercial suppliers (Leyan reagent, Aladdin) and were used without further purification. All the reactions were carried out using a round bottom flask in a nitrogen atmosphere in anhydrous solvents. ^{1}H and ^{13}C NMR spectra were obtained in $CDCl_3$ on a WJGS-037 Bruker AVANCE Ⅲ 400 MHz NMR spectrometer, using tetramethyl silane (TMS) as the internal standard. Mass spectra were recorded on an Agilent 1290 Infinity. UV-vis absorbance and photoluminescence (PL) spectra were recorded on a Shimadzu UV-3600 and a Fluorescence spectrophotometer F-380A, respectively. Photoluminescence quantum efficiencies (PLQYs) were measured using Quantaurus-QY C11347-11.

Bromination of **2,7-di-*tert*-butylpyrene**

The bromination was carried out with 6 equiv. of bromine in the presence of iron powder at room temperature for 1h. A mixture of 4,5,9-tribromo-2,7-di-*tert*- butylpyrene and 4,5,9,10-tetrabromo-2,7-di-*tert*-butylpyrene was obtained as a white powder, the ratio of these two compounds is 1:9 (calculated by ^{1}H NMR spectroscopy).

4,5,9-Tribromo-2,7-di-*tert*-butylpyrene (TriBrPy): ^{1}H NMR (400 MHz, $CDCl_3$): δ_H = 8.84 (s, 1H, Py-*H*) ,8.77 (s, 1H, Py-*H*), 8.71 (s, 1H, Py-*H*), 8.44 (s, 1H, Py-*H*), 8.20 (s, 1H, Py-*H*), 1.59 (s, 18H, *t*-Bu);

4,5,9,10-Tetrabromo-2,7-di-*tert*-butylpyrene (TetraBrPy): ^{1}H NMR (400 MHz, $CDCl_3$): δ_H = 8.87 (s, 4H, Py-*H*), 1.62 (s, 18H, *t*-Bu).

Synthesis of compounds **TriPhPy** and **TetraPhPy**

A mixture of **TetraBrPy** doped with **TriBrPy** (500 mg, 0.8 mmol), 4-methoxy phenylboronic acid (972 mg, 6.4 mmol) in toluene (140 mL) and ethanol (80 mL) at room temperature was stirred under argon, and K_2CO_3 (2 M, 20 mL) solution and $Pd(PPh_3)_4$ (92 mg, 0.08 mmol) were added. After the mixture was stirred for 30 min at room temperature under nitrogen, the mixture was heated to 90 °C for 24 h with stirring. After cooling to room temperature, the mixture was quenched with water, extracted with CH_2Cl_2 (3 × 100 mL), washed with water. The organic extracts were dried with $MgSO_4$ and evaporated. The residue was separated by column chromatography eluting with (hexane/CH_2Cl_2, 3:1) and then recrystallization from (hexane/CH_2Cl_2, 1:1) to give **TriPhPy** and **TetraPhPy** as a white solid.

TriPhPy: **2,7-Di-*tert*-butyl-4,5,9-tri(4-methoxyphenyl)pyrene** was obtained as a white powder (40 mg, 79 %); M.p. > 300 °C; ^{1}H NMR (400 MHz, $CDCl_3$): δ_H = 8.27 (s, 1H Py-*H*), 8.17 (s, 1H Py-*H*), 8.00 (s, 1H Py-*H*), 7.91 (s, 1H Py-*H*), 7.89 (s, 1H Py-*H*), 7.64 (d, *J* = 7.6 Hz, 2H, Ar-*H*), 7.18 (d, *J* = 7.6Hz, 4H, Ar-*H*), 7.12 (d, *J* = 8.0 Hz, 2H, Ar-*H*), 6.86 (d, *J* = 8.0 Hz, 4H, Ar-*H*), 3.96 (s, 3H, OMe-*H*), 3.85 (s, 6H, OMe-*H*), 1.42 (s, 9H, *t*-Bu), 1.32 (s, 9H, *t*-Bu); ^{13}C NMR (100 MHz, $CDCl_3$): δ 159.0, 157.9, 148.6, 148.0, 139.0, 137.8, 137.6, 133.7, 132.3, 131.6, 131.3, 131.2, 130.4, 130.0, 127.9, 122.8, 122.1, 121.9, 120.8, 113.8, 113.1, 113.1, 55.4, 55.2, 35.4, 35.3, 31.8. FAB-MS: m/z: calcd for $C_{45}H_{44}O_3$ 632.3290 [M^+]; found 632.3278[M^+].

TetraPhPy: **2,7-Di-*tert*-butyl-4,5,9,10-tetrakis(4-methoxyphenyl)pyrene** was obtained as colourless prisms (188 mg, 35 %). M.p. > 300 °C; ^{1}H NMR (400 MHz, $CDCl_3$): δ_H = 7.89 (s, 4H), 7.19 (d, *J* = 8.4 Hz, 8H, Ar-*H*), 6.86 (d, *J* = 8.4 Hz, 8H, Ar-*H*), 3.85 (s, 12H, OMe-*H*), 1.25 (s, 18H, *t*-Bu); ^{13}C NMR (100 MHz, $CDCl_3$): δ

157.9, 148.0, 137.6, 133.3, 132.5, 132.3, 131.2, 121.8, 113.1, 77.2, 55.1, 31.7. FAB-MS: m/z: calcd for $C_{52}H_{50}O_4$ 738.3709 [M^+]; found 738.3723[M^+].

Author Contributions

Hua-Long Li: Investigation, Formal analysis, Writing-review&editing. Jing-Yi Cao: Investigation, Formal analysis, Writing-review&editing. Ze-Dong Yu: Investigation, Formal analysis. Guang Yang: Investigation, Formal analysis. Zeng-Min Xue: Software computational studies. Chuan-Zeng Wang: Conceptualization, Investigation, Writing-review&editing. Wen-Xuan Zhao: Investigation, Formal analysis. Yi Zhao: Software-computational studies, Writing-review&editing. Carl Redshaw: Writing-review&editing. Takehiko Yamato: Conceptualization, Writing-review&editing

Conflicts of interest

The authors declare that they have no known competing financial interests or personal relationships that could have appeared to influence the work reported in this paper.

Acknowledgements

This work was performed under the Cooperative Research Program of "Network Joint Research Center for Materials and Devices (Institute for Materials Chemistry and Engineering, Kyushu University)". We would like to thank the Natural Science Foundation of Shandong Province (Grant No. ZR2019BB067), this research used resources of the Advanced Light Source, which is a DOE Office of Science User Facility under contract no. DE-AC02-05CH11231. CR thanks the University of Hull for support.

References

1 R. K. Sharma, S. Yadav, S. Dutta, H. B. Kale, I. R. Warkad, R. Zboril, R. S. Varma and M. B. Gawande, Silver nanomaterials: synthesis and (electro/photo) catalytic applications, *Chem. Soc. Rev.*, 2021, **50**, 11293–11380.

2 M. Roldan, E. Perez-Reinado, F. Castillo and C. Moreno-Vivian, Reduction of polynitroaromatic compounds: the bacterial nitroreductases, *FEMS Microbiol. Rev.*, 2008, **32**, 474–500.

3 Y. F. Xue, H. Bai, B. Peng, B. Fang, J. Baell, L. Li, W. Huang and N. H. Voelcker, Stimulus-cleavable chemistry in the field of controlled drug delivery, *Chem. Soc. Rev.*, 2021, **50**, 4872–4931.

4 H. Yi, G. M. Zeng, C. Lai, D. L. Huang, L. Tang, J. L. Gong, M. Chen, P. Xu, H. Wang, M. Cheng, C. Zhang and W. P. Xiong, Environment-friendly fullerene separation methods, *Chem. Eng. J.*, 2017, **330**, 134–145.

5 H. Yi, D. L. Huang, L. Qin, G. M. Zeng, C. Lai, M. Cheng, S. J. Ye, B. Song, X. Y. Ren and X. Y. Guo, Selective prepared carbon nanomaterials for advanced photocatalytic application in environmental pollutant treatment and hydrogen production, *Appl. Catal., B*, 2018, **239**, 408–424.

6 D. L. Huang, X. L. Yan, M. Yan, G. M. Zeng, C. Y. Zhou, J. Wan, M. Cheng and W. J. Xue, Graphitic carbon nitride-based heterojunction photoactive nanocomposites: applications and mechanism insight, *ACS Appl. Mater. Interfaces*, 2018, **10**, 21035–21055.

7 X. M. Gong, D. L. Huang, Y. G. Liu, G. M. Zeng, R. Z. Wang, J. J. Wei, C. Huang, P. Xu, J. Wan and C. Zhang, Pyrolysis and reutilization of plant residues after phytoremediation of heavy metals contaminated sediments: for heavy metals stabilization and dye adsorption, *Bioresour. Technol.*, 2018, **253**, 64–71.

8 T. K. Naqvi, A. K. Srivastava, M. M. Kulkarni, A. M. Siddiqui and P. K. Dwivedi, Silver nanoparticles decorated reduced graphene oxide (rGO) SERS sensor for multiple analytes, *Appl. Surf. Sci.*, 2019, **478**, 887–895.

9 Y. J. Gao, F. J. Chu, W. W. Chen, X. Z. Wang and Y. J. Pan, Arc-Induced Nitrate Reagent Ion for Analysis of Trace Explosives on Surfaces Using Atmospheric Pressure Arc Desorption/Ionization Mass Spectrometry, *Anal. Chem.*, 2022, **94**, 5463–5468.

10 L. Duflin, X. M. Wang and J. Stoesz, Detection of volatile organic compounds in froth multiphase systems from oil sands operations using a headspace GC–MS method, *Energy Fuels*, 2017, **31**, 11925–11931.

11 L. M. Han, J. Kaesler, C. Peng, T. Reemtsma and O. J. Lechtenfeld, Online counter gradient LC-FT-ICR-MS enables detection of highly polar natural organic matter fractions, *Anal. Chem.*, 2021, **93**, 1740–1748.

12 S. F. Chen, X. Q. Chen, T. T. Xia and Q. Ma, A novel electrochemiluminescence sensor for the detection of nitroaniline based on the nitrogen-doped graphene quantum dots, *Biosens. Bioelectron.*, 2016, **85**, 903–908.

13 T. Jadoon, F. Ullah, T. Mahmood and K. Ayub, Silver cluster decorated graphene nanoflakes for selective and accurate detection of nitroaniline isomers; DFT calculations, *Mater. Sci. Semicond. Process.*, 2021, **134**. 106023–106015.

14 E. McGillicuddy, I. Murray, S. Kavanagh, L. Morrison, A. Fogarty, M. Cormican, P. Dockery, M. Prendergast, N. Rowan and D. Morris, Silver nanoparticles in the environment: Sources, detection and ecotoxicology, *Sci. Total Environ.*, 2017, **575**, 231–246.

15 Y. Liu, X. Xu, Y. Wei, Y. S. Chen, M. Gao, Z. J. Zhang, C. L. Si, H. P. Li, X. Y. Ji and J. J. Liang, Tailoring silver nanowire nanocomposite interfaces to achieve superior stretchability, durability, and stability in transparent conductors, *Nano Lett.*, 2022, **22**, 3784–3792.

16 P. Y. Wu, Y. H. Liu, Y. Li, M. Jiang, X. L. Li, Y. H. Shi and J. Wang, A cadmium(ii)-based metal–organic framework for selective trace detection of nitroaniline isomers and photocatalytic degradation of methylene blue in neutral aqueous solution, *J. Mater. Chem. A.*, 2016, **4**, 16349–16355.

17 F. P. Kinik, A. Ortega-Guerrero, D. Ongari, C. P. Ireland and B. Smit, Pyrene-based metal organic frameworks: from synthesis to applications, *Chem. Soc. Rev.*, 2021, **50**, 3143–3177.

18 G. Q. Lin, H. M. Ding, D. Q. Yuan, B. S. Wang and C. Wang, A pyrene-based, fluorescent three-dimensional covalent organic framework , *J. Am. Chem. Soc.*, 2016, **138**, 3302–3305.

19 G. Das, B. P. Biswal, S. Kandambeth, V. Venkatesh, G. Kaur, M. Addicoat, T. Heine, S. Verma and R. Banerjee, Chemical sensing in two dimensional porous covalent organic nanosheets, *Chem. Sci.*, 2015, **6**, 3931–3939.

20 X. G. Liu, D. L. Huang, C. Lai, G. M. Zeng, L. Qin, H. Wang, H. Yi, B. S. Li, S. Y. Liu, M. M. Zhang, R. Deng, Y. K. Fu, L. Li, W. J. Xue and S. Chen, Recent advances in covalent organic frameworks (COFs) as a smart sensing material, *Chem. Soc. Rev.*, 2019, **48**, 5266–5302.

21 Z. Li, J. R. Askim and K. S. Suslick, The optoelectronic nose: colorimetric and fluorometric sensor arrays, *Chem. Rev.*, 2019, **119**, 231–292.
22 T. Naghdi, S. Faham, T. Mahmoudi, N. Pourreza, R. Ghavami and H. Golmohammadi, Phytochemicals toward Green (Bio)sensing, *Acs Sensors*, 2020, **5**, 3770–3805.
23 X. C. Sun, Y. Wang and Y. Lei, Fluorescence based explosive detection: from mechanisms to sensory materials, *Chem. Soc. Rev.*, 2015, **44**, 8019–8061.
24 H. S. Jung, P. Verwilst, W. Y. Kim and J. S. Kim, Fluorescent and colorimetric sensors for the detection of humidity or water content, *Chem. Soc. Rev.*, 2016, **45**, 1242–1256.
25 Y. F. Zhao, H. Zeng, X. W. Zhu, W. G. Lu and D. Li, Metal–organic frameworks as photoluminescent biosensing platforms: mechanisms and applications, *Chem. Soc. Rev.*, 2021, **50**, 4484–4513.
26 C.L. Zhong, J. W. Qiu, Y. J. Tong, M Liu, X. Y. Xiong, and Y. Gao, High selective inner filter effect based method and its application in 2,4,6-trinitrophenol detection *Dyes Pigm.*, 2022, **206**, 110654.
27 M. Wang, L. Guo and D. P. Cao, Porous organic polymer nanotubes as luminescent probe for highly selective and sensitive detection of Fe^{3+}, *Science China-Chemistry*, 2017, **60**, 1090–1097.
28 F. P. Kinik, A. Ortega-Guerrero, D. Ongari, C. P. Ireland and B. Smit, Pyrene-based metal organic frameworks: from synthesis to applications, C*hem. Soc. Rev.*, 2021, **50**, 3143–3177.
29 T. M. Figueira-Duarte and K. Mullen, Pyrene-based materials for organic electronics, *Chem. Rev.*, 2011, **111**, 7260–7314.
30 X. Feng, J. Y. Hu, C. Redshaw and T. Yamato, Functionalization of pyrene to prepare luminescent materials—typical examples of synthetic methodology, *Chem-Eur J.*, 2016, **22**, 11898–11916.
31 X. Wang, J. Zhang, X. Mao, Y. Liu, R. Li, J. Bai, J. Zhang, C. Redshaw, X. Feng and B. Z. Tang, Intermolecular hydrogen-bond-assisted solid-state dual-emission molecules with mechanical force-induced enhanced emission, *J. Org. Chem.*, 2022, **87**, 8503–8514.
32 C. Z. Wang, X. Feng, Z. Kowser, C. Wu, T. Akther, M. R. J. Elsegood, C. Redshaw and T. Yamato, Pyrene-based color-tunable dipolar molecules: Synthesis, characterization and optical properties, *Dyes Pigm.*, 2018, **153**, 125–131.
33 R. Liu, H. Ran, Z. Zhao, X. Yang, J. Zhang, L. Chen, H. Sun and J. Y. Hu. Synthesis and Optical Properties of Donor–Acceptor-Type 1,3,5,9-Tetraarylpyrenes: Controlling Intramolecular Charge-Transfer Pathways by the Change of π-Conjugation Directions for Emission Color Modulations, *ACS Omega*, 2018, **3**, 5866-5875.
34 J. Y. Hu, M. Era, M. R. J. Elsegood and T. Yamato, Synthesis and Photophysical Properties of Pyrene‐Based Light‐Emitting Monomers: Highly Pure‐Blue‐Fluorescent, Cruciform‐Shaped Architectures, *Eur. J. Org. Chem.*, 2010, **1**, 72-79.
35 J. Y. Hu, X.-L. Ni, X. Feng, M. Era, M. R. J. Elsegood, S. J. Teat and T. Yamato, Highly emissive hand-shaped π-conjugated alkynylpyrenes: Synthesis, structures, and photophysical properties, *Org. Biomol. Chem.*, 2012, **10**, 2255-2262.
36 J. M. Casas-Solvas, J. D. Howgego and A. P. Davis. Synthesis of substituted pyrenes by indirect methods, *Org. Biomol. Chem.*, 2014, **12**, 212-232.
37 Z. D. Yu, J. Y. Cao, H. L. Li, G. Yang, W. X. Zhao, C. Z. Wang, S. H. Chen, M. R. J. Elsegood, C. Redshaw and T. Yamato, Crystallization-induced emission enhancement of alkyl chain-dependent pyrene-based luminogens: Visual detection of nitro-explosives, *J. Lumin.*, 2023, **253**, 119439.
38 S. Y. Kim, M. J. Kim, M. Ahn, K. M. Lee and K. R. Wee, Systematic energy band gap control of pyrene based donor-acceptor-donor molecules for efficient chemosensor, *Dyes Pigm.*, 2021, **191**, 109362.
39 X. Feng , N. Seto, C. Z. Wang, T. Matsumoto, J. Tanaka, X. F. Wei, M. R. J. Elsegood, L. Horsburgh, C. Redshaw and T. Yamato, Extended π-Conjugated Pyrene Derivatives: Structural, Photophysical and Electrochemical Properties, *ChemistrySelect*, 2016, **1**, 1926–1932.
40 J. X Chen, H. Wang, X. Zhang, Y. F. Xiao, K. Wang, L. Zhou, Y. Z. Shi, J. Yu, C. S. Lee and X. H. Zhang, Using fullerene fragments as acceptors to construct thermally activated delayed fluorescence emitters for high-effciency organic light-emitting diodes, *Chem. Eng. J.*, 2022, **435**, 134731.
41 Z. D. Yu, J. Y. Cao, H. L. Li, G. Yang, Z. M. Xue, L. Jiang, J. Y. Yu, C. Z. Wang, X. Y. Liu, C. Redshaw and T. Yamato, Structure-controlled intramolecular charge transfer in asymmetric pyrene-based luminogens: synthesis, characterization and optical properties, *New J. Chem.*, 2022, **46**, 16394–16400.
42 C. Z. Wang, Z. D. Yu, W. X. Zhao, K. Yang, Y. Noda, Y. Zhao, X. Feng, M. R. Elsegood, S. J. Teat, C. Redshaw and T. Yamato, Pyrene-fused hexaarylbenzene luminogens: Synthesis, characterization, and aggregation-induced emission enhancement, *Dyes Pigm.*, 2021, **192**, 109452.
43 C. Z. Wang, R. Zhang, K. Sakaguchi, X. Feng, X. Yu, M. R. J. Elsegood, S. J. Teat, C. Redshaw and T. Yamato, Two‐Photon‐Absorption Properties of Pyrene‐Based Dipolar D-π-A Fluorophores, *ChemPhotoChem*, 2018, **2**, 749–756.
44 J. Mei, N. L. Leung, R. T. Kwok, J. W. Lam and B. Z. Tang, Aggregation-induced emission: together we shine, united we soar! *Chem. Rev.*, 2015, **115**, 11718–11940.
45 S. Grimme, J. Antony, S. Ehrlich and H. Krieg, A consistent and accurate ab initio parametrization of density functional dispersion correction (DFT-D) for the 94 elements H-Pu, *The Journal of chemical physics*, 2010, **132**, 154104.
46 J. Liu, Y. Zhang, K. Zhang, J. Fan, C. K. Wang and L. Lin, Bicolor switching mechanism of multifunctional light-emitting molecular material in solid phase, *Org. Electron.*, 2019, **71**, 212–219.
47 Z. D. Yu, X. X. Dong, J. Y. Cao, W. X. Zhao, G. H. Bi, C. Z. Wang, T. Zhang, S. Rahman, P. E. Georghiou, J. B. Lin and T. Yamato, Substituent effects on the intermolecular interactions and emission behaviors in pyrene-based mechanochromic luminogens, *J. Mater Chem. C*, 2022, **10**, 9310–9318.
48 M. M. Islam, Z. Hu, Q. Wang, C. Redshaw and X. Feng, Pyrene-based aggregation-induced emission luminogens and their applications, *Mater. Chem. Front.*, 2019, **3**, 762–781.
49 V. Bhalla, H. Arora, H. Singh and M. Kumar, Triphenylene derivatives: chemosensors for sensitive detection of nitroaromatic explosives, *Dalton Trans.*, 2013, **42**, 969–974.
50 D. Zhao and T. M. Swager, Sensory responses in solution vs solid state: a fluorescence quenching study of poly (iptycenebutadiynylene) s, *Macromolecules*, 2005, **38**, 9377–9384.
51 P. Das, G. Chakraborty and S. K. Mandal, Comprehensive Structural and Microscopic Characterization of an Azine–Triazine-Functionalized Highly Crystalline Covalent Organic Framework and Its Selective Detection of Dichloran and 4-Nitroaniline, *ACS Appl. Mater. Interfaces*, 2020, **12**, 10224−10232.

